RESULTS ON NEUTRINO OSCILLATIONS FROM 400 DAYS OF SUPER-KAMIOKANDE DATA

Yoshitaka Itow

Kamioka Observatory

Institute for Cosmic Ray Research, University of Tokyo, Higashi-Mozumi

Kamioka, Gifu, 506-12, Japan

Representing the Super-Kamiokande Collaboration[1]

ABSTRACT

The Super-Kamiokande experiment, using the world's largest underground water Cherenkov detector, has been running since April 1, 1996. The total live time for the analysis has reached more than 350 days. The latest results on atmospheric neutrinos, solar neutrinos, and related topics are reported.

1 Introduction

The Super-Kamiokande detector is a 50,000-ton water Cherenkov detector located at a depth of 2,700 meters water equivalent in the Kamioka mine in Japan. A schematic view of the detector is shown in Fig. 1. The detector cavity is 42 m in height and 39 m in diameter, and is filled with 50,000 tons of pure water. The fiducial mass for the measurement of solar and atmospheric neutrino interactions is 22,000 tons, which is more than 20 times larger than that of Kamiokande. It consists of two layers of detector. The inner tank is 33.8 m in diameter and 36.2 m high. Cherenkov photons radiated by relativistic charged particles are detected by 11,146 50-cm photomultiplier tubes (PMT's), instrumented on all surfaces of the inner detector. The outer layer, approximately 2-m thick, is used as an anticounter where 1,885 20-cm PMT's are instrumented. The anticounter is useful for identifying entering cosmic-ray muons and for reducing gamma rays or neutrons from the surrounding rock. Pulse-height and timing information from each PMT is recorded and used in the data analysis.

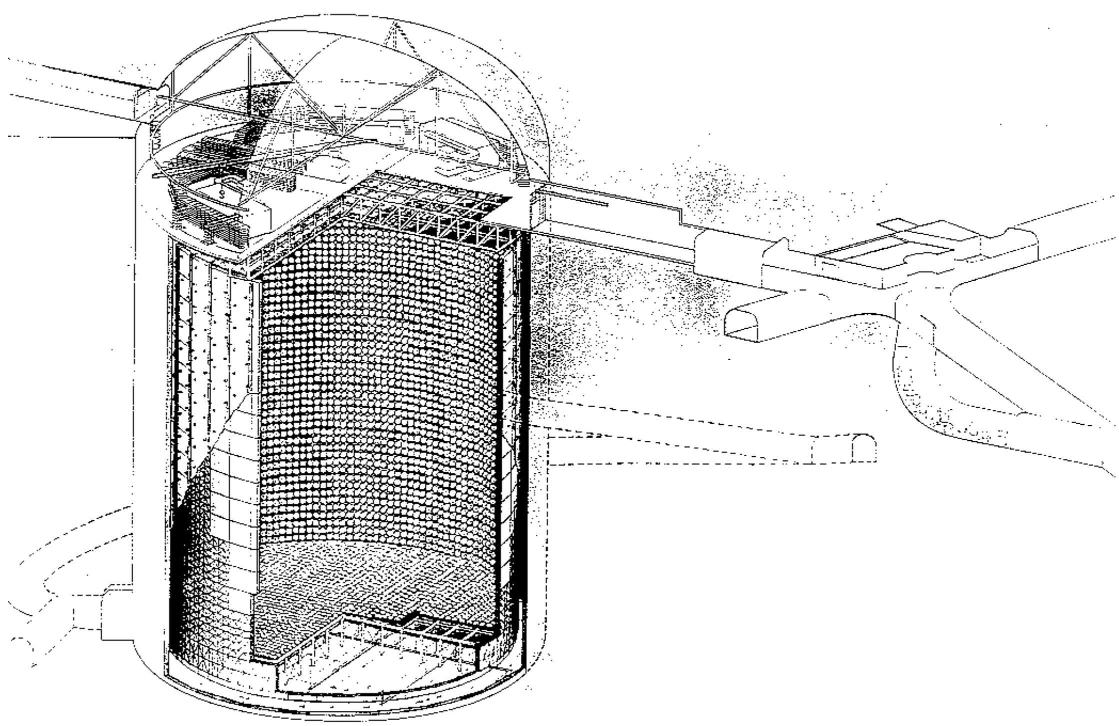

Figure 1: The schematic view of the Super-Kamiokande detector.

Super-Kamiokande has been successfully operating without any serious problems since April 1, 1996. The detector has been alive 85% of the time. Most of the dead time is due to calibrations. The cumulative live time of operation reached more than 500 days in the fall of 1997. The transparency of water is about 80 m, as measured using electrons from μ decay. The trigger threshold had been about 5.6 MeV for electrons at 50% efficiency from the beginning of the experiment. It has been set to about 4.6 MeV since May 1997 to collect a much lower energy data sample. The concentration of Rn in the water is less than 5 m Bq/m^3, which is two orders of magnitude lower than that in Kamiokande. The total live time of the data sample for analysis of solar neutrinos, up-going muons, atmospheric neutrinos, and proton decay has reached more than 300 days. Now it is time to obtain conclusive results in neutrino oscillation studies using this large statistics data set. In the following sections, new results in solar neutrino and in atmospheric neutrino analyses are presented.

2 Solar Neutrinos

The sun maintains its luminosity by the energy of nuclear fusion reactions. Thus the sun emits low-energy (E$_\nu \leq 15$ MeV) electron neutrinos (ν_e) that are products of the nuclear processes inside the sun. Our understanding of those processes is reflected in the standard solar model (SSM). The flux and spectrum of neutrinos corresponding to each nuclear process are well-predicted by the SSM. Figure 2 shows the energy spectrum of the solar neutrino flux on the earth calculated by the SSM of Bahcall and Pinsonneault in 1995 (BP-95) (Ref. 2). Also shown are the energy thresholds of five current existing solar neutrino experiments, the Homestake experiment,[3] Kamiokande,[4] SAGE,[5] GALLEX,[6] and the present experiment, Super-Kamiokande,[7] in the same figure.

The first observation of solar neutrinos was achieved in the early 1970s by Davis *et al.* by using the following reactions: $^{37}\mathrm{Cl} + \nu_e \rightarrow\ ^{37}\mathrm{Ar} + e^-$ ($E_\nu \geq$ 0.814 MeV). Their obtained results have shown a significant deficit of the yield compared to predictions based on various versions of the SSM. The SAGE and GALLEX experiments used the following reactions: $^{71}\mathrm{Ga} + \nu_e \rightarrow\ ^{71}\mathrm{Ge} + e^-$ ($E_\nu \geq 0.233$ MeV). Those experiments can detect much lower energy neutrinos produced via the "p-p" chain that maintains most of the sun's luminosity. The obtained results are about half of what was expected. Kamiokande has performed the first real-time measurement of solar neutrinos by using the water Cherenkov technique. Solar neutrinos can be detected through neutrino-electron scattering, $\nu e \to \nu e$. The electron energy, direction, and time of the reaction are measured. The obtained result was about 40% of the expectation.

Table 1: Results from the current five experiments and the SSM[2] BP-95 predictions on the solar neutrino flux. Here the unit is SNU for ^{37}Cl and ^{71}Ga and 10^6 $\nu/\mathrm{cm}^2/\mathrm{sec}$ for $e^-(H_2O)$ targets, respectively, where SNU means "solar neutrino unit" defined by 1 SNU $= 10^{-36}$ ν captures per atom per second.

Target (Exp.)	Data	SSM (BP-95)	Data/SSM$^{(*)}$
^{71}Ga(SAGE)	$69 \pm 10^{+5}_{-7}$	137^{+8}_{-7}	$0.504^{+0.082}_{-0.089}$
^{71}Ga(GALLEX)	$69.7 \pm 6.7^{+3.9}_{-4.5}$	137^{+8}_{-7}	$0.509^{+0.057}_{-0.059}$
^{37}Cl(Homestake)	$2.55 \pm 0.14 \pm 0.14$	$9.3^{+1.2}_{-1.4}$	0.273 ± 0.021
$e^-(H_2O$, Kamiokande)	$2.80 \pm 0.19 \pm 0.33$	$6.62^{+0.93}_{-1.12}$	0.423 ± 0.058
$e^-(H_2O$, Super-Kam.)$^{(**)}$	$2.37^{+0.06+0.09}_{-0.05-0.07}$	$6.62^{+0.93}_{-1.12}$	$0.358^{+0.017}_{-0.013}$

(∗) Experimental errors only. Statistical and systematic errors are added in quadrature.
(∗∗) Preliminary.

The flux measurements are summarized in Table 1. All the experiments show significantly lower flux than that from the SSM prediction, while the detection methods and the energy thresholds of the measurement are different from each other. It is hard to explain all the existing results consistently within the SSM. The solar neutrinos that are expected to be detected in the Homestake experiment are about 80% from ^{8}B neutrinos and about 15% from ^{7}Be neutrinos, while only ^{8}B neutrinos can be detected by the water Cherenkov detectors. The obtained Data/SSM in the Homestake experiment is about 1/3, while it is about one half in Kamiokande. This difference suggests almost no contribution from ^{7}Be neutrinos in the Homestake data. On the other hand, the contributions of "p-p" neutrinos, ^{7}Be neutrinos, and ^{8}B neutrinos in the data sample of the Ga experiments are expected to be about 50%, 30%, and 10%, respectively. The flux of "p-p" neutrinos is constrained by the total luminosity of the sun. It again may suggest a strong suppression of ^{7}Be neutrinos. These results from the existing experiments hint at a possible distortion of the energy spectrum of solar neutrinos, which can be explained by the hypothesis of $\nu_e \to \nu_x$ oscillations. The distance between the earth and the sun is $\sim 10^{11}$ m and $E_\nu \sim 10$ MeV, so that typically E/L is 10^{-10} eV^2. If Δm^2 is substantially larger than 10^{-10} eV^2, solar neutrinos with any energy are fully oscillated in the case of vacuum oscillations. Thus, Data/SSM of all the existing experiments should be the same and the different Data/SSM among the experiments are hardly explained. One of the scenarios is that Δm^2 and $\sin^2 2\theta$ eventually take "good" values, for example (Δm^2, $\sin^2 2\theta$) $\sim$ (10^{-10}, 1), to explain all the results. This scenario is called the "just-so oscillation." Figure 3, taken from Ref. 8, shows the 95% C.L. allowed regions of the just-so solution in (Δm^2, $\sin^2 2\theta$) space. The other attractive scenario which could explain all of the experimental results is matter-enhanced oscillations of solar neutrinos, so-called MSW oscillation.[9] Figure 4, taken from Ref. 8, shows the 95% C.L. allowed regions of MSW solution in (Δm^2, $\sin^2 2\theta$) space. There are two domains of allowed regions, so-called small angle solutions and large angle solutions. It is predicted that the energy spectrum of solar neutrinos would be distorted in the case of the small angle solution. On the other hand, the Day/Night effect, that is, a difference between day and night flux, would be observed in the case of the large angle solution. Real-time measurement of solar neutrinos is indispensable to detect these effects, which would be strong evidence of MSW oscillation. Super-Kamiokande, with its large fiducial mass, can provide a huge statistical sample for these measurements.

The solar neutrino data of 374.2 live days presented here covers the period from May 31, 1996 through October 20, 1997. First, cosmic ray muons and decay electrons are discarded from the data sample using the total energy deposited in the detector and the time difference of the events. The vertex position of the ν-e scattering and the direction of the electrons have been reconstructed by using arrival-time information of Cherenkov photons on the PMT's of the inner detector. The energy of the electron has been determined from the number of hit PMT's in a 50 ns window. The energy scale, the energy resolution, the angular resolution, and the vertex position resolution are calibrated mainly with the electron beam from a LINAC system. The LINAC system can produce an electron beam of 5–16 MeV injected to various positions in the detector. The energy, angular, and position resolutions for 8.6 MeV electrons are 16%, 27 degrees, and 85 cm, respectively. The uncertainty of the absolute energy scale is $\pm 1\%$. Both the position dependence and time variance of the energy scale are $\pm 1\%$, which has been checked with a

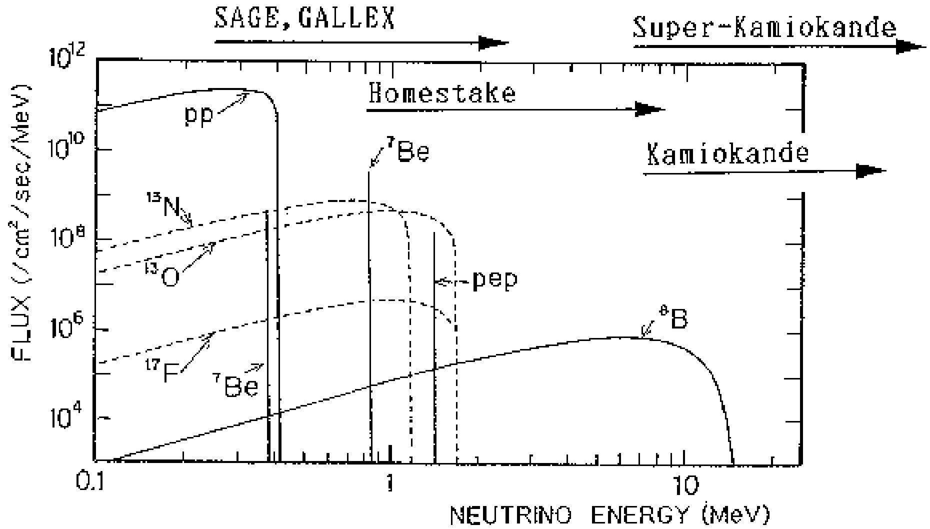

Figure 2: The energy spectrum of the solar neutrino flux. Also shown are the energy thresholds of the existing solar neutrino experiments.

Ni-Cf source by using the reaction Ni(n,γ)Ni. To eliminate the background events due to activity from surrounding rocks, we required that the distance of the vertex from the inner detector wall be more than 2 m. This corresponds to 22.5 kt as a fiducial mass. Another background due to the activity from nuclear fragments produced by μ spallation has been reduced by checking the distance and time interval between an event and a prior cosmic ray μ event. Finally, the distribution of electron direction relative to the sun has been obtained for the events where the electron energy is between 6.5 and 20 MeV, as shown in Fig. 5. The number of obtained solar neutrino events is $4951.8^{+117.9}_{-111.3}$(stat.)$^{+444}_{-154}$(syst.) which corresponds to $2.37^{+0.06}_{-0.05}$(stat.)$^{+0.09}_{-0.07}$(syst.) $\times\ 10^6/\mathrm{cm}^2/\mathrm{s}$ as a ^{8}B-neutrino flux. The obtained Data/SSM is $0.358^{+0.009}_{-0.008}$(stat.)$^{+0.014}_{-0.010}$(syst.). The present total flux result is consistent with the previous result observed in Kamiokande. Note that the number of obtained solar neutrinos by Super-Kamiokande in one and a half years of operation is more than eight times larger than that by Kamiokande in seven years of operation.

The flux difference between day and night is expressed as:

$$(\mathrm{Day} - \mathrm{Night})/(\mathrm{Day}\ +\ \mathrm{Night}) = -0.031 \pm 0.024(stat.) \pm 0.014(syst.).$$

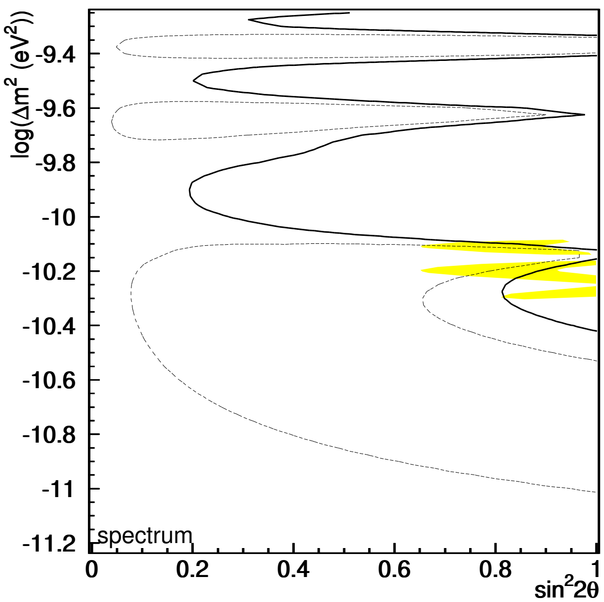

Figure 3: The 95% C.L. allowed region of just-so oscillations in the fit by Hata and Langacker[8] is shown by the shaded region. Also shown are the preliminary 95% C.L. and 99% C.L. contours in the just-so region from the spectrum analysis, without the flux constraint in Super-Kamiokande. The region inside the dashed lines are allowed at 95% C.L., and the regions to the right of the solid line are excluded at 99% C.L. using the spectrum analysis.

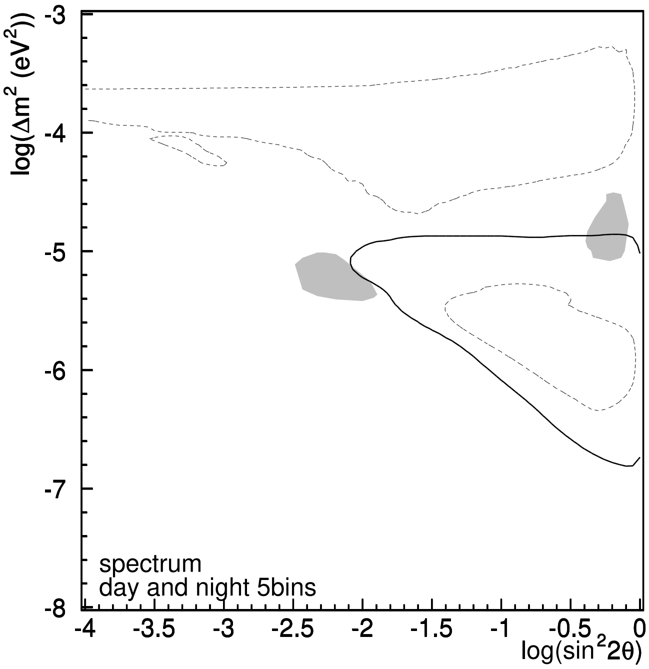

Figure 4: The 95% C.L. allowed regions for MSW oscillations in (Δm^2, $\sin^2 2\theta$) space in the fit by Hata and Langacker[8] are shown by the shaded regions. Also shown is the 95% C.L. excluded region for MSW oscillations analysis, without using the flux constraint. The Day/Night analysis excludes the region inside of the solid line, and the spectrum analysis excludes the regions inside the dashed lines.

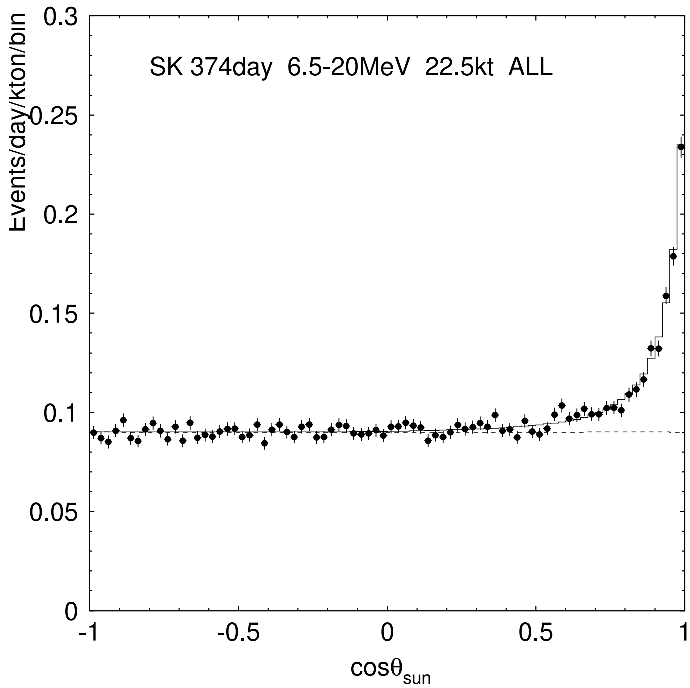

Figure 5: Preliminary solar neutrino data from the Super-Kamiokande experiment in 374.2 days of observation. A clear excess of events near $\cos\theta_{sun} = 1$ is seen. The shape of the excess distribution is reproduced well by the MC simulation with a ^{8}B flux of $0.358 \times$ SSM.

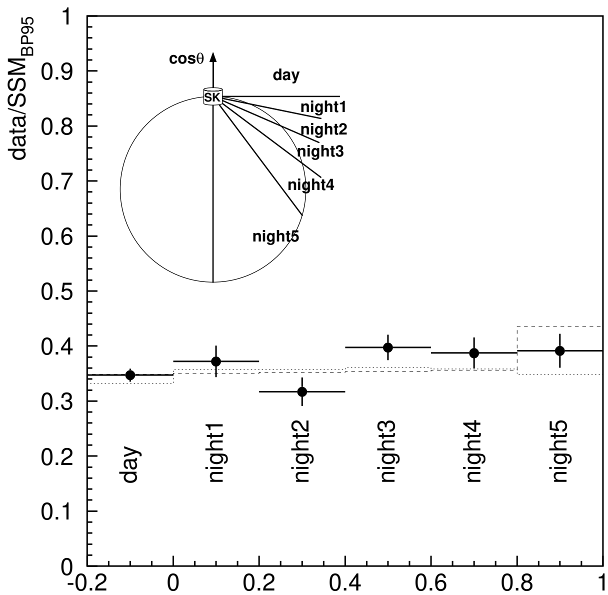

Figure 6: Preliminary results on the Day/Night effect. Error bars are statistical only. The night data is divided into five bins. Night 1 is the horizontal direction and night 5 is the vertical direction. The histogram with dashed lines is the expected variation of the typical large angle solution and the histogram with dotted lines is that of the typical small angle solution (see text).

Within the statistics, there is, so far, no evidence for the Day/Night effect. Figure 6 shows the solar neutrino flux in day and night periods. The night and day flux are subdivided into five bins according to the angle between the direction to the sun and the nadir of the detector. The five-binned histograms expected from MSW oscillation with typical parameters in the small mixing solution, $(\Delta m^2, \sin^2 2\theta) = (6.31 \times 10^{-6}, 9.12 \times 10^{-3})$, and in the large angle solution, $(\Delta m^2, \sin^2 2\theta) = (2.82 \times 10^{-5}, 0.66)$, are also shown in the figure. The data seems to agree with no Day/Night effect, but also to the Day/Night effect with some parameters of the large angle solution. An analysis of the implications for the MSW oscillations has been performed for the five-binned Day/Night result shown in Fig 6. This analysis is a model-independent analysis, since only the variation of the ^{8}B-neutrino flux between day and night is used. The excluded region at 95% C.L. from the analysis of obtained results in the Day/Night effect are plotted in Fig. 4. The presented results have excluded the lower Δm^2 region in the large angle solution.

Figure 7 shows Data/SSM as a function of electron energy. The inside error bars show statistical errors, and outside bars show the systematic error, mainly due to uncertainty in the energy scale and energy resolution. These systematic errors are fully correlated to the energy of the electrons. Also shown is the expected spectrum of the typical small angle solution, $(\Delta m^2, \sin^2 2\theta) = (6.31 \times 10^{-6}, 9.12 \times 10^{-3})$, and the typical just-so oscillation, $(\Delta m^2, \sin^2 2\theta) = (7.08 \times 10^{-11}, 0.83)$. There appears to be no significant distortion in the obtained spectrum. However, it is interesting that possible distortions of the spectra, by neutrino oscillations for example, as shown in the figure, also agree with data and give even better χ^2 for the fitting. The model-independent implication of the energy spectrum has been performed in the MSW parameter region and in the just-so parameter region. We have not used the constraint of the ^{8}B-neutrino flux from the SSM for the analysis, due to its 20% uncertainty. The contour plots for MSW oscillation and for just-so oscillation are shown in Fig. 4 and in Fig. 3, respectively. The absence of significant distortion of the energy spectrum excludes some regions in both of the parameter spaces. Because of a good fit of the spectrum in the just-so region, the 95% C.L. allowed region appears as shown in Fig. 3, though the no-oscillation hypothesis is still allowed at 99% C.L.

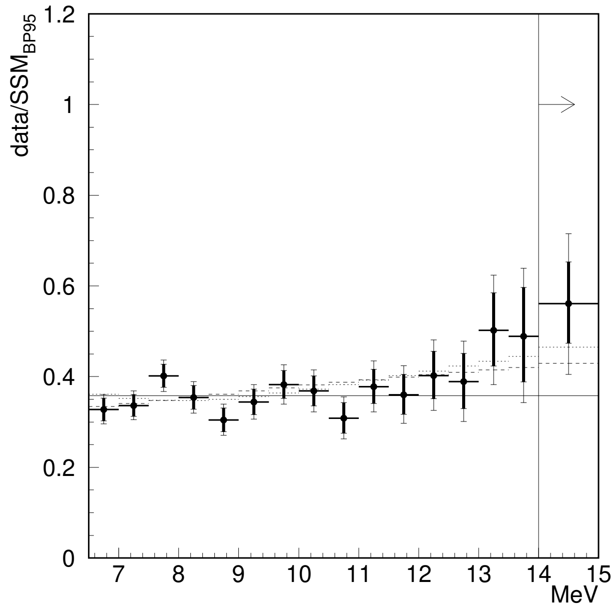

Figure 7: Preliminary plot of Data/SSM as a function of electron energy from Super-Kamiokande. The right-most bin shows the data with electron energy more than 14 MeV. Inner error bars are statistical and outer bars are the systematic errors added linearly with the statistical ones. The dashed histogram is the expected spectrum of the typical small angle solution and the dotted histogram is that of the typical just-so solution (see text).

3 Atmospheric Neutrinos

Atmospheric neutrinos are produced by the decay of pions or kaons produced by the interaction of the primary component of cosmic rays in the atmosphere. The typical altitude where atmospheric neutrinos are produced is 10 km so that the typical flight length of neutrinos is $\sim$ 10 km for down-going ones and $\sim 10^4$ km for up-going ones. The ν_μ/ν_e ratio of the atmospheric neutrino flux below a few GeV is roughly two, since π decay is dominant and the $\pi \to \mu \to e$ decay chain is $\pi^\pm \to \mu^\pm + \nu_\mu(\bar{\nu}_\mu), \mu^\pm \to e^\pm + \nu_e(\bar{\nu}_e) + \bar{\nu}_\mu(\nu_\mu)$. (Hereafter, ν represents $\nu + \bar{\nu}$.) It goes up to more than two for higher energy neutrinos, since high-energy μ's hit the ground before they decay. The total flux of atmospheric neutrinos has been calculated by several models. The uncertainty in the flux is about 20%, while the uncertainty in the ν_μ/ν_e ratio is 5% in the region below a few GeV. To cope with the detection efficiency of the detector, the "double ratio R" defined as

$$R = \frac{(\nu_\mu/\nu_e)_{data}}{(\nu_\mu/\nu_e)_{MC}} \tag{1}$$

is often used. If $(\nu_\mu/\nu_e)_{data}$ is consistent with the prediction, R should take the value unity.

In recent years, there have been several measurements of the ν_μ/ν_e ratio with water Cherenkov detectors, IMB-3 (Refs. 10 and 11), and Kamiokande (Ref. 12), and with tracking-type detectors, NUSEX (Ref. 13), Frejus (Ref. 14), and Soudan-2 (Ref. 15). See Table 2. Two water Cherenkov experiments, Kamiokande and IMB, have obtained consistent results which are substantially smaller than unity. The anomaly in the μ/e ratio can be interpreted as possible neutrino oscillation, for example, $\nu_\mu \to \nu_e$ or $\nu_\mu \to \nu_\tau$. On the other hand, the results of NUSEX and Frejus seem to be consistent with $R = 1$, while their statistics are not sufficient for conclusive results. Furthermore, recent data from Soudan-2 agree with the data from the water Cherenkov detectors, although the value of unity is still allowed at the 2σ level. Though the theoretical uncertainty of the absolute flux and interaction cross sections of neutrinos is large, they should cancel in the double ratio. Hence, the small double ratio can be considered as possible evidence of $\nu_\mu \to \nu_e$ or $\nu_\mu \to \nu_\tau$ oscillations.

Another indication of the oscillation of atmospheric neutrinos is the distortion of the zenith angle distribution of the neutrino flux. The flux of atmospheric neutrinos depends on the zenith angle. This dependence is caused by a differ-

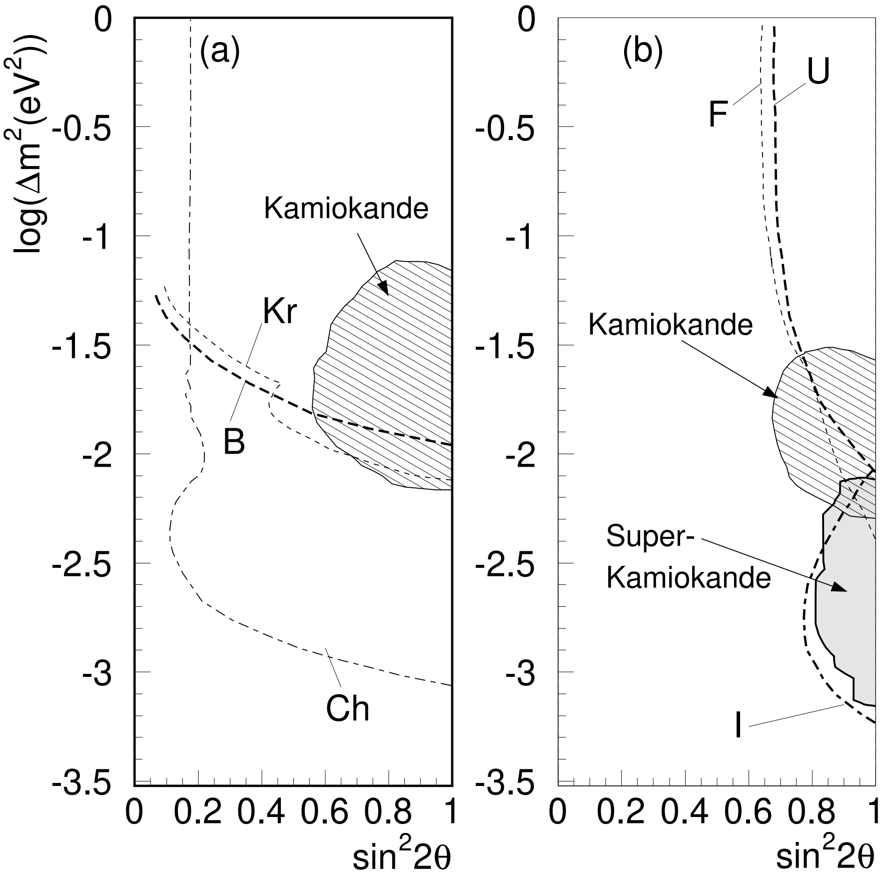

Figure 8: Allowed regions (90% C.L.) in the (Δm^2, $\sin^2 2\theta$) space (a) for ν_μ–ν_e oscillation and (b) for ν_μ–ν_τ oscillation. Regions with diagonal lines show the allowed regions obtained by Kamiokande.[12] The shaded region in (b) is the preliminary allowed region by Super-Kamiokande. Other lines indicate that the regions above and to their right are excluded: B, Bugey reactor experiment;[16] Kr, Krasnoyarsk reactor experiment;[17] Ch, Chooz reactor experiment;[18] F, Frejus fully-contained atmospheric neutrinos;[14] U, compilation of upward through-going muons data;[19] I, IMB upward-stopping muons.[20] Super-Kamiokande's analysis on ν_μ–ν_e oscillation was not ready in time for this plot.

Table 2: Experimental results on the atmospheric (ν_μ/ν_e) ratio.

Exp.	Data		MC		$(\mu/\mathrm{e})_{data}/(\mu/\mathrm{e})_{MC}$
	e-like	μ-like	e-like	μ-like	
NUSEX	18	32	20.5	36.8	$0.99^{+0.35}_{-0.25} \pm ?$
Frejus	75	125	81.4	136.2	$1.00 \pm 0.15 \pm 0.08$
Soudan-2	79.1	54.6			$0.67 \pm 0.15^{+0.04}_{-0.06}$
IMB-3 (sub-GeV)	325	182	257.3	268.0	$0.54 \pm 0.05 \pm 0.12$
(multi-GeV)	25	47	30.8	41.2	$1.40 \pm 0.66 \pm 0.21$
Kamiokande (sub-GeV)	248	234	227.6	356.8	$0.60^{+0.06}_{-0.05} \pm 0.05$
(multi-GeV)	98	135	66.5	162.2	$0.57^{+0.08}_{-0.07} \pm 0.07$
Super-Kam. (sub-GeV)$^{(*)}$	983	900	812.2	1218.3	$0.61^{+0.029}_{-0.028} \pm 0.049$
(multi-GeV)$^{(*)}$	218	176	182.7	229.0	$0.64^{+0.069}_{-0.062} \pm 0.097$
(PC)$^{(*)}$	—	200	—	244.8	$0.67^{+0.059}_{-0.054} \pm 0.081^{(**)}$

(∗) Preliminary.

(∗∗) The double ratio is for the combined sample of FC and PC events.

ence in the effective thickness of the atmosphere. Hence, the shape of the zenith angle distribution should be symmetric for up-going versus down-going neutrinos. A typical E/L for atmospheric neutrinos of 1 GeV, for example, is 10^{-1} for down-going and 10^{-4} for up-going. Therefore, a distortion of the zenith angle distribution would be clear evidence of neutrino oscillations. Only the Kamiokande experiment has reported the zenith angle distribution of the neutrino flux for the time being.[12] They reported a possible distortion of the zenith angle distribution in the multi-GeV sample (E_ν higher than roughly 1 GeV), which suggests neutrino oscillations with $\Delta m^2 \sim 10^{-2}$ eV^2 and with a large mixing angle as shown in Fig. 8. Much more data are needed to establish the oscillation of atmospheric neutrinos. Super-Kamiokande can collect data with large statistics, which are indispensable to test the oscillation hypothesis and to derive the oscillation parameters from the double ratio and zenith angle distribution.

3.1 Fully-Contained and Partially-Contained Events

We have analyzed fully-contained (FC) events of 414.2 live days (25.5 kton-years) and partially-contained (PC) events of 370.8 live days (22.8 kton-years). In an FC event, all the charged particles are contained in the inner detector and the total energy of the event is fully reconstructed. In a PC event, one charged particle, usually a muon, escapes from the inner detector and deposits energy into the outer detector. To separate an FC event from a PC event, we have required that the total number of hits in a spatial cluster in the outer detector be less than ten. Both FC and PC events have been doubly scanned by physicists to eliminate background events due to detector noise. Then, the vertex positions of the neutrino interaction and Cherenkov rings have been reconstructed automatically by a computer. The vertex position resolution is estimated to be 30 cm for single-ring FC events. The angular resolution of single-ring FC events is estimated to be three degrees. Finally, a 2-m fiducial cut has been applied for events in both the FC and PC samples. Total visible energy cuts, $E_{vis} \geq 30$ MeV and $E_{vis} \geq 350$ MeV, have been applied for the FC and the PC sample, respectively. The accuracy of the absolute energy scale is estimated to be $\pm$ 2.4% based on several calibration sources: cosmic ray through-going muons, stopping muons, muon-decay electrons, the invariant mass of π^0's produced by neutrino interactions, Ni-Cf source calibration, and the 5–16 MeV LINAC. The momentum of particles is determined from the total number of photoelectrons within a 70-degree half-angle cone relative to the track direction. The estimated momentum resolution for electrons and muons is $2.5\%/\sqrt{E} + 0.5\%$ and 3%, respectively, where E is the energy of the electron in GeV. After applying the cuts, the number of neutrinos is 3,462 for the FC sample and 200 for the PC sample. The number of events per day is 8.4 for the FC sample and 0.54 for the PC sample.

In the FC events, single-ring events have been selected. Figure 9 shows a typical single-ring "e-like" event and a "μ-like" event. There is a difference between the shapes of the rings in the figure, since a Cherenkov ring from an electromagnetic cascade causes a more diffuse photon distribution than that from a muon. The particle identification (PID) method, which uses the distribution of Cherenkov photons in a ring as well as the opening angle of the ring, is applied to distinguish muons from electrons. Figure 10 shows the result of PID for single-ring FC events. The two peaks corresponding to μ and e are clearly separated in these distributions. The probability of misidentification deduced from Monte Carlo is less than 0.5% for the single-ring FC sample. The PC events are regarded as μ-like events, since 97% of the PC events are caused by charged current ν_μ interactions.

Table 2 shows the final results for two different energy regions, namely sub-GeV and multi-GeV, according to the definition of the selection criteria used in

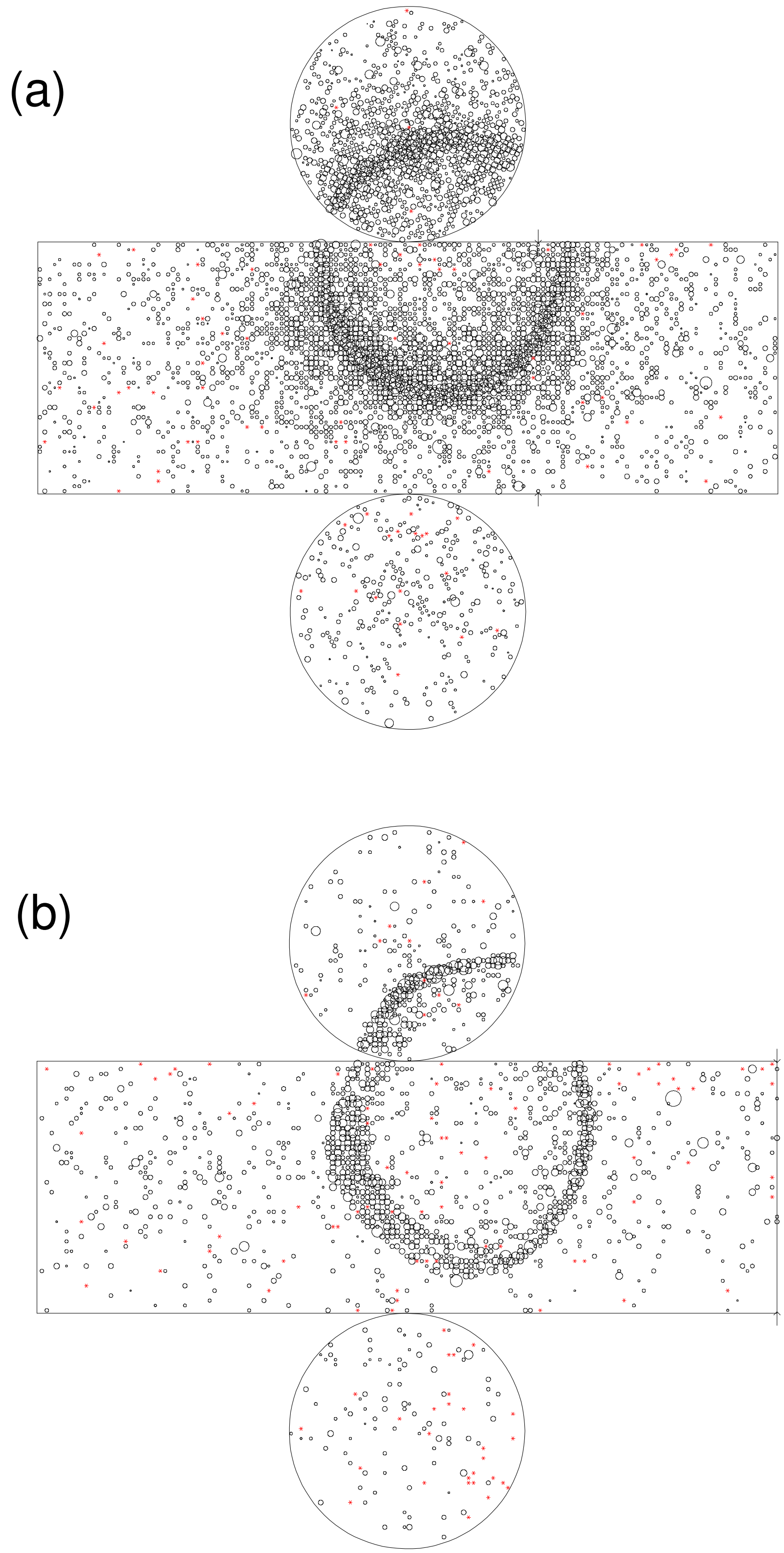

Figure 9: Typical samples of an (a) one-ring e-like event and (b) one-ring μ-like event.

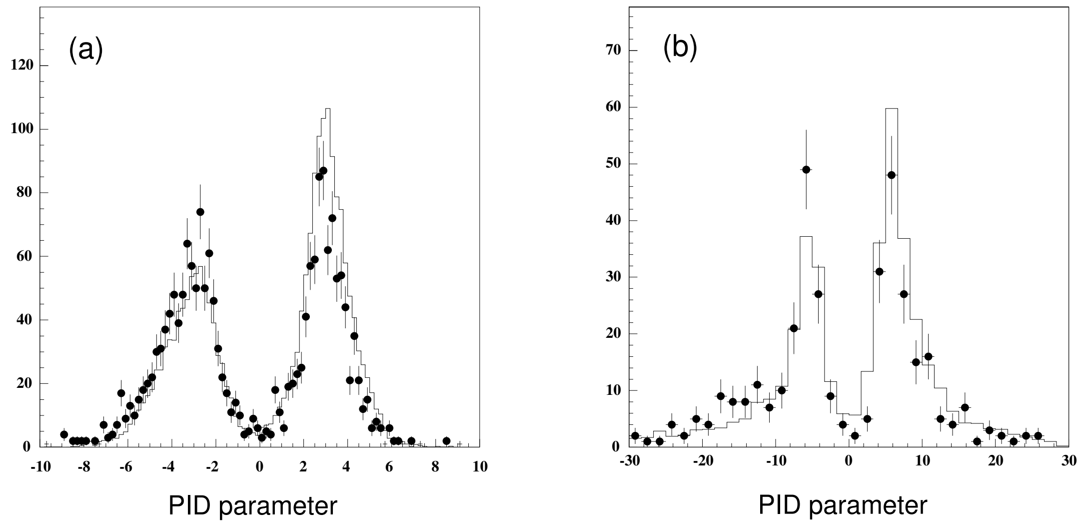

Figure 10: Distribution of the PID parameter for μ-like events (PID < 0) and for e-like events (PID > 0) in (a) a sub-GeV sample and in (b) a multi-GeV sample. The closed circles and histograms are for the data and for Monte Carlo events, respectively.

Kamiokande. The sub-GeV sample is the subset of FC events where (1) $E_{vis} <$ 1.33 GeV, (2) $P_e >$ 100 MeV/c for e-like events, and (3) $P_\mu >$ 200 MeV/c for μ-like events. In the sub-GeV sample, the number of single-ring e-like and μ-like events are 983 and 900, respectively, while the expected numbers using Honda's flux[21] are 812.2 and 1218.3 for the single-ring e-like and μ-like events, respectively. The multi-GeV sample is the subset of FC events with $E_{vis} \geq 1.33$ GeV. The number of single-ring e-like and μ-like events are 218 and 176, respectively, while the expected numbers are 182.7 and 229.0. The number of PC events is 200, while the expected number is 244.8. These numbers are summarized in Table 2. As shown above, Super-Kamiokande observed small double ratios for both the sub-GeV and the multi-GeV energy sample. The double ratios are $0.611^{+0.029}_{-0.028} \pm 0.049$ and $0.665^{+0.059}_{-0.054} \pm 0.081$ for the sub-GeV FC sample and combined sample of multi-GeV FC and PC, respectively. The obtained double ratios in Super-Kamiokande are therefore inconsistent with unity and are consistent with the previous results of water Cherenkov experiments. Thus, the atmospheric neutrino anomaly has been established.

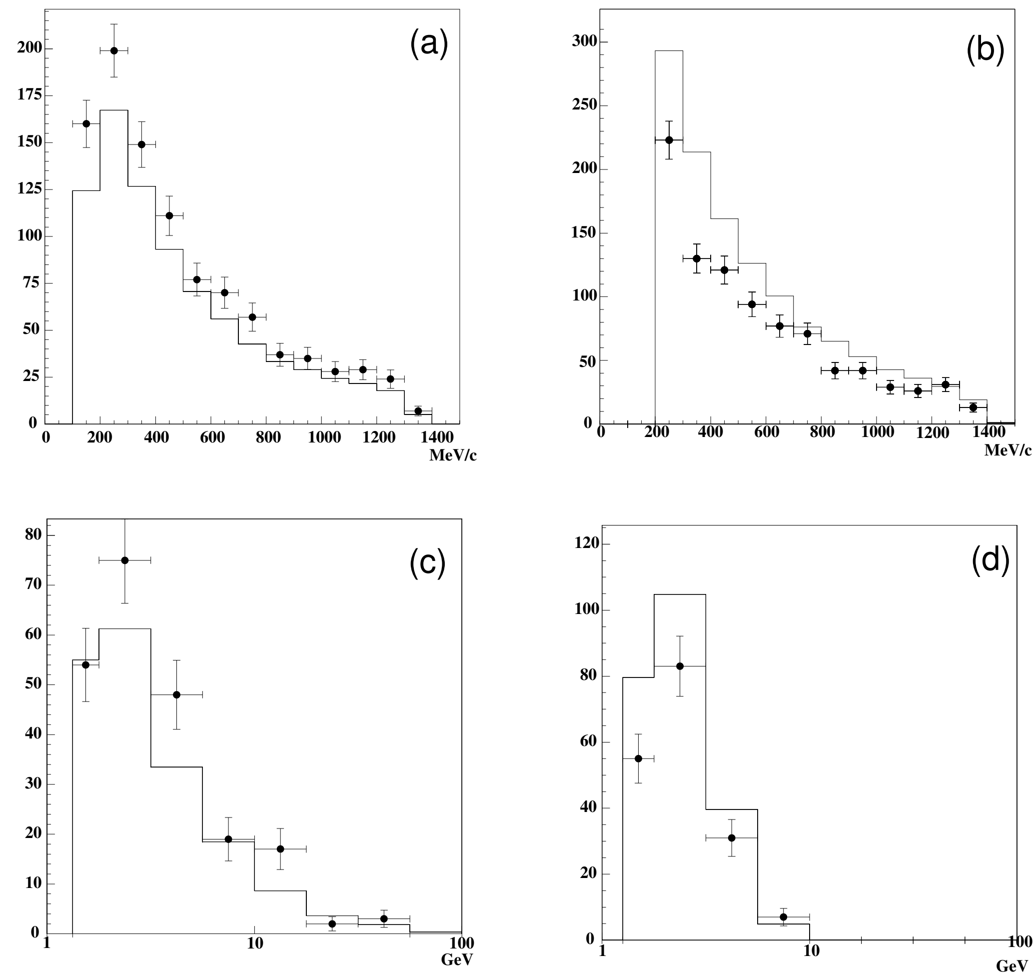

Figure 11: Momentum distribution for (a) e-like and (b) μ-like events in the sub-GeV sample and (c) e-like and (d) μ-like events in the multi-GeV sample from Super-Kamiokande. The histograms show the MC prediction.

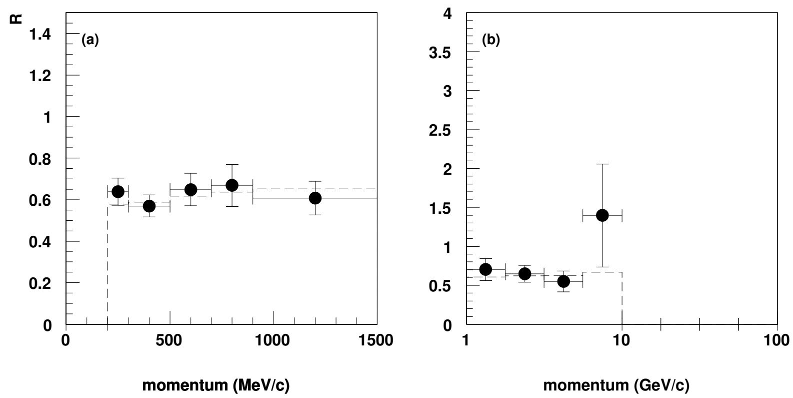

Figure 12: The momentum dependence of the double ratio R for (a) sub-GeV and (b) multi-GeV. The closed circles show the data. The histograms with a dashed line show the expected distribution with $\nu_\mu \to \nu_\tau$ oscillation in the case of (Δm^2, $\sin^2 2\theta$) = (5×10^{-3}, 1).

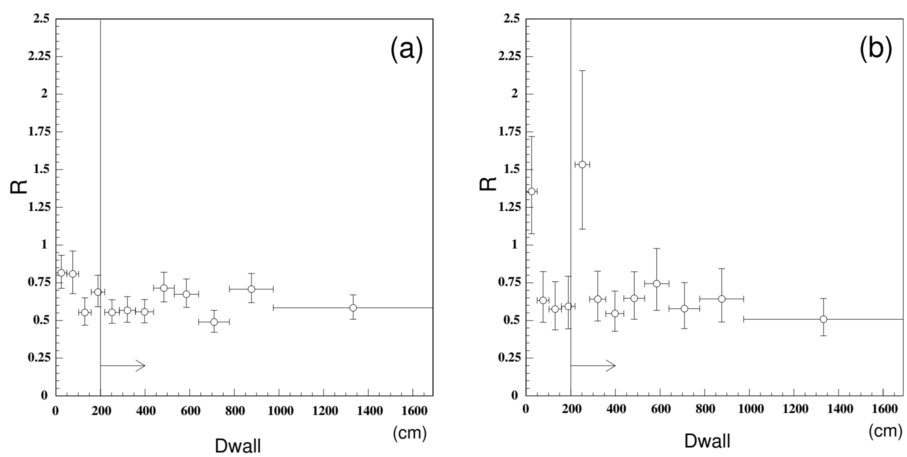

Figure 13: The double ratio R in each D_{wall} bin for (a) the sub-GeV and (b) the multi-GeV sample. The 2-m fiducial volume cuts are also shown.

Figure 11 shows the momentum distribution for the FC events. One can see that the shape of the distributions for the e-like and μ-like events is reproduced well by the Monte Carlo. We cannot determine whether a ν_μ deficit or a ν_e excess takes place due to the 25% uncertainty in absolute normalization coming from uncertainty in the neutrino flux and neutrino interaction cross sections. The deficit (excess) of events in the muons (electrons) of the data, however, cannot be explained within the 5% uncertainty of the expected μ/e ratio. Figure 12 shows the double ratio versus lepton momentum in both of the samples. It appears that the small double ratio does not depend strongly on the momentum. Figure 13 shows the double ratio versus D_{wall} distance from the inner wall. Each bin of D_{wall} is chosen to give the same fiducial mass. It is clear that the double ratio is not dependent on the vertex position. This proves that the obtained small double ratios are not due to contamination from any kind of incoming particles like cosmic ray muons or neutrons from the rock.

The higher energy neutrinos have the better angular correlation with the lepton produced via a charged current interaction. For example, the angle between the neutrino and the lepton is roughly 20 degrees in the multi-GeV sample. The direction of neutrinos can be measured by using the direction of a single ring. Figure 14 shows the zenith angle distribution of μ-like events and e-like events in sub-GeV and multi-GeV + PC samples, together with Monte Carlo expectations. Significantly, a large deficit of upward-going neutrinos is observed in the multi-GeV μ-like sample. Note that any systematic effects due to the cross section and neutrino flux calculation are canceled in the symmetry of the zenith angle distribution, and cannot explain this large distortion. The hypothesis of neutrino oscillations can naturally explain this asymmetry. A preliminary oscillation analysis assuming $\nu_\mu \to \nu_\tau$ oscillation has been made. The 90% C.L. allowed region is shown in Fig. 8. Although the suggested region is slightly lower in Δm^2 than that of Kamiokande, a region of overlap with the Kamiokande result appears at around 5×10^{-3} eV^2.

3.2 Results for Upward-Going Muons

Another indication of neutrino oscillations can be derived from upward-going muon data. The upward-going muons are produced by charged current ν_μ interactions in the rock near the detector. If the energy of the muons is larger

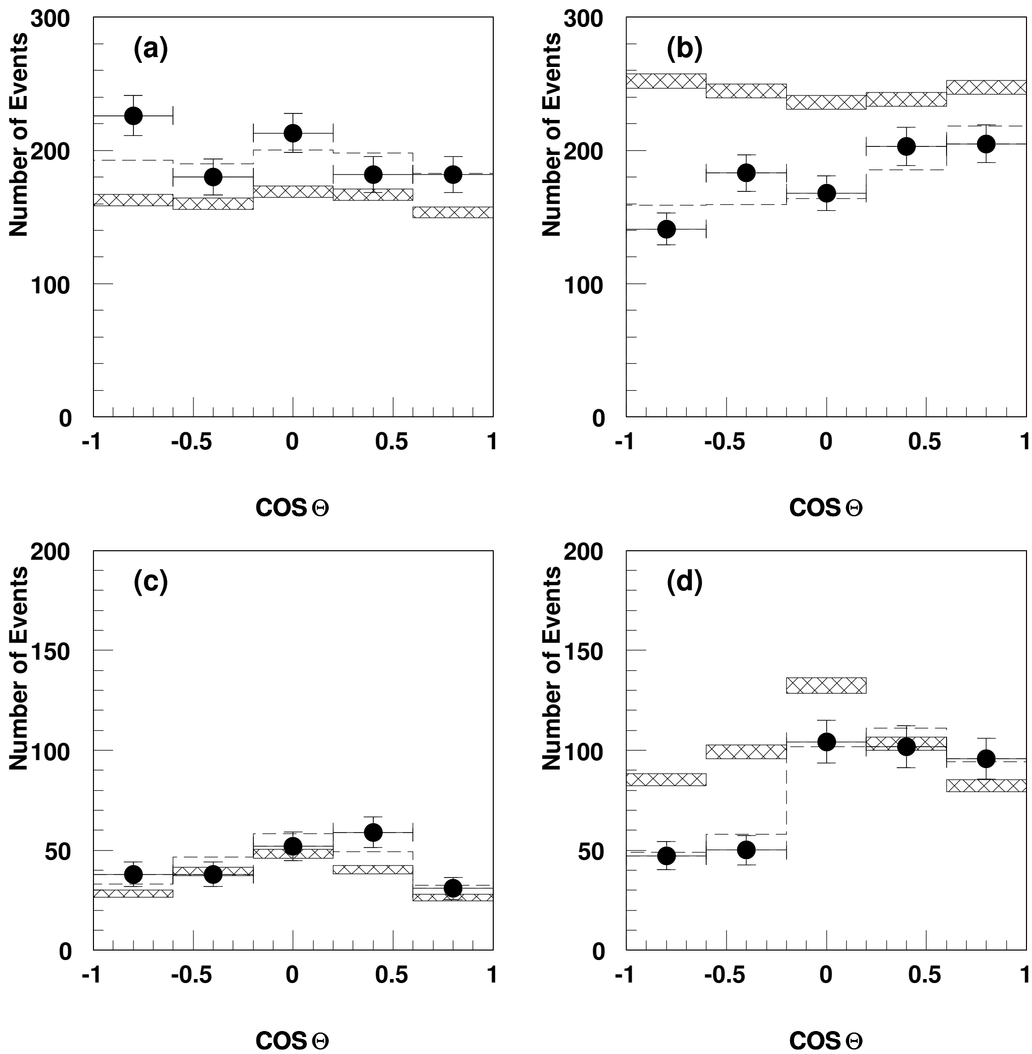

Figure 14: The double ratio R as a function of zenith angle for (a) sub-GeV e-like, (b) sub-GeV μ-like, (c) multi-GeV e-like, and (d) multi-GeV μ-like events. Histograms with a solid line show the expectation from the Monte Carlo without oscillations. The hatched boxes show the errors due to Monte Carlo statistics. Histograms with a dashed line show the expectation with $\nu_\mu \to \nu_e$ oscillation with $(\Delta m^2, \sin^2 2\theta) = (5 \times 10^{-3}, 1)$. Down-going particles correspond to $\cos\theta = 1$.

than several GeV, they pass through the detector. These are called "upward-through-going muons." The typical neutrino energy is on the order of 100 GeV for upward-through-going muons.

Upward-through-going muons have been selected from a data sample of 362 live days. All the directions and entering positions of muons have been reconstructed automatically by a program, then later by manual fitting to measure them more precisely. Cosmic ray muons, which are the main background events, are easily rejected by applying the zenith angle cut ($\cos\theta_z \leq 0$). The path length of the muon track in the inner detector has been required to be more than 7 m. This corresponds to a 1.7 GeV cut. The total observed number of upward-through-going muons is 409 in 362 live days. The expected number of upward-through-going muons from a calculation is 445 ± 89. It is hard to compare the obtained number of up-going muons to the expected one, since the absolute number has about 20% uncertainty due to the flux of atmospheric neutrinos and the cross section. However, a distortion of the zenith angle distribution would be free from such systematics and could be evidence of neutrino oscillations, just as in the vertex-contained event data.

Figure 15 shows the zenith angle distribution obtained from Kamiokande and from Super-Kamiokande, together with the expectation. The closed circles and open circles show the data of Kamiokande and of Super-Kamiokande, respectively. The data agree well. The expected distributions in the cases of no oscillation and of oscillation with $(\Delta m^2, \sin^2 2\theta) = (5 \times 10^{-3}, 1)$ are also shown; the no oscillation case is represented by thick solid and dashed lines for Super-Kamiokande and Kamiokande, respectively; the oscillation case, by thin solid and dashed lines. The plotted histograms are best-fit ones, allowing for a 20% uncertainty in the absolute normalization. The data of the two experiments are consistent with either expectation, with no oscillation within errors; i.e., the statistics so far are not enough. However, it is interesting that the hypothesis of $\nu_\mu \rightarrow \nu_x$ oscillation with the parameter suggested by the contained events data, for example $(\Delta m^2, \sin^2 2\theta) = (5 \times 10^{-3}\ \mathrm{eV}^2, 1)$, agrees well with the data, or fits even better. Apparently, much higher statistics data and further study of systematic errors are needed to give a decisive answer for neutrino oscillations.

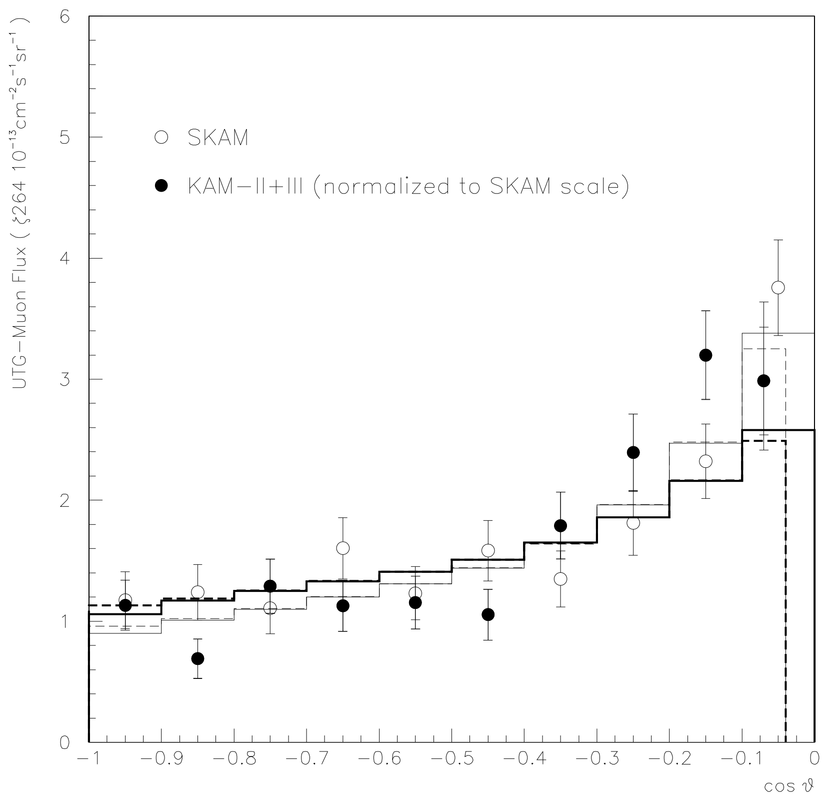

Figure 15: The zenith angle distribution of upward-through-going muons from Kamiokande (full circle) and Super-Kamiokande (open circle). Histograms show the expected distributions from no oscillation (thick solid and dashed lines for Super-Kamiokande and Kamiokande, respectively) and from $\nu_\mu - \nu_\tau$ oscillation with $\Delta m^2 = 5 \times 10^{-3}\,\mathrm{eV}^2$ and $\sin^2 2\theta = 1$ (thin solid and dashed lines for Super-Kamiokande and Kamiokande, respectively). The results and expected lines for Kamiokande were multiplied by a factor of 0.819 to scale its geometrical effect to Super-Kamiokande. The expected histograms are the best-fit ones, allowing for an absolute scale uncertainty of 20%.

4 Future Long-Baseline Experiments at KEK

The effect of neutrino oscillation suggested by the atmospheric neutrino data can be studied by long-baseline neutrino oscillation experiments using a high-intensity ν_μ beam. One of the possible experiments is the one between the KEK-PS (proton synchrotron) and Super-Kamiokande (called K2K).[22] It has a baseline length of 250 km and the average energy of the ν_μ beam is roughly 1.5 GeV, so that it is just sensitive to the $\Delta m^2 \sim 10^{-2}$ eV^2 region suggested by the Super-Kamiokande data.

The 12 GeV proton beam is extracted from the KEK-PS within a 1 μsec interval every two seconds. π^+'s produced by 12 GeV protons are focused by horn magnets and decay into $\mu^+\nu_\mu$ in the 200 m long decay tunnel. The fraction of ν_e in the beam is less than 1%. There are two kinds of beam monitors, the π monitor and the μ monitor, in the decay tunnel. The π monitor downstream of the horn magnets is a gas Cherenkov detector which measures the emission angle of Cherenkov photons produced by the π beam with various gas pressures. This monitor provides information about the distribution of momentum and the divergence of the π beam. The μ monitor downstream of the beam dump measures the profile of μ's from the π decays. Those two monitors are useful to understand the properties of the ν_μ beam.

There is a front detector 300 m away from the target to measure the initial flux of the ν_μ beam. The front detector consists of the Fine Grain Detector and a 1,000-ton water Cherenkov detector. The Fine Grain Detector is a tracking-type detector which consists of a "sandwich" of a scintillating fiber tracker and a water layer as a target. The aim of the detector is to measure the absolute ν_μ flux with 5% accuracy by choosing the quasi-elastic charged current interaction. The 1,000-ton water Cherenkov detector has the same configuration as Super-Kamiokande. The aim of the detector is to study the detector response characteristic of the water Cherenkov technique, using the neutrino beam well-measured by the Fine Grain Detector.

The number of charged current interactions expected at Super-Kamiokande is about 350 for 10^{20} protons on target (POT) in two years of running. This experiment can search for $\nu_\mu \to \nu_e$ and $\nu_\mu \to \nu_\tau$ independently. $\nu_\mu \to \nu_e$ oscillation can be observed as an appearance of e-like events at Super-Kamiokande. $\nu_\mu \to \nu_\tau$ oscillation can be observed as distortion of the ν_μ energy spectrum, which can

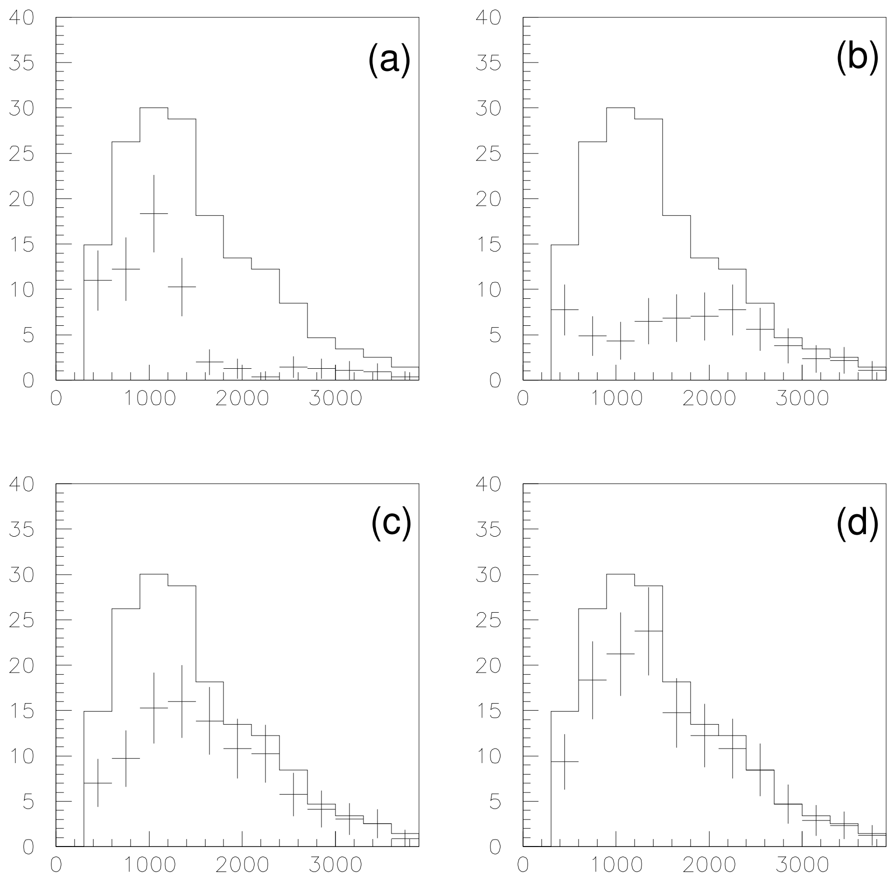

Figure 16: The expected energy distribution of ν_μ at Super-Kamiokande reconstructed from single-ring μ-like events. The histograms show the data without oscillation. The crosses show the data in the case of $\nu_\mu - \nu_\tau$ oscillation with $\sin^2 2\theta = 1$ and (a) with $\Delta m^2 = 10^{-2}$ eV^2, (b) with $\Delta m^2 = 5 \times 10^{-3}$ eV^2, (c) with $\Delta m^2 = 3 \times 10^{-3}$ eV^2, and (d) with $\Delta m^2 = 2 \times 10^{-3}$ eV^2.

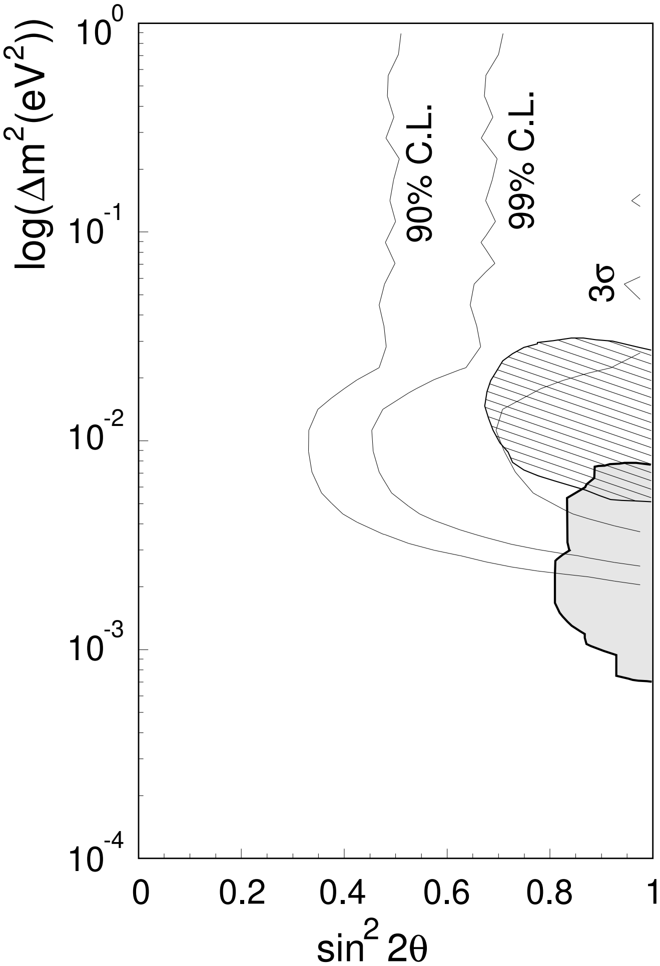

Figure 17: The sensitivity plot in (Δm^2, $\sin^2 2\theta$) space for the search for ν_μ disappearance with 10^{20} POT by using the neutrino energy spectrum analysis. Contours at the 90% C.L., 99% C.L., and 3 σ levels are shown. Also shown are the allowed regions from the Kamiokande and Super-Kamiokande results.

be reconstructed from single-ring μ-like events at Super-Kamiokande. Figure 16 shows the reconstructed energy spectrum of ν_μ's with no oscillation and with oscillation. One can see the significant distortion in the spectrum in the case of oscillation with the range of Δm^2 values suggested by the atmospheric neutrino data. The sensitivity for the ν_μ disappearance measurement is plotted in Fig. 17. The region where Δm^2 is greater than 3×10^{-3} eV^2 and $\sin^2 2\theta$ is greater than 0.6 can be explored in this experiment.

The construction of the new neutrino beamline was started in 1996. The installation of the front detector will start in October 1998. The first neutrino beam will be extracted in January 1999. The physics run will start in April 1999 and continue for two to three years. It will give a conclusive result for the oscillation parameters and modes.

5 Conclusion

Super-Kamiokande is the largest underground water Cherenkov detector dedicated to the detection of neutrinos and proton decays. Super-Kamiokande has been running continuously since April 1, 1996 and has collected neutrino data with much greater statistics than has been achieved so far by any underground neutrino experiment.

The preliminary solar neutrino results reported here are based on 374 live days of data. The observed flux of solar neutrinos is apparently smaller than the expectation of the SSM, and consistent with the previous results of Kamiokande. The Day/Night difference is consistent with zero within error. This result partially excludes the lower Δm^2 region in the large-angle solution of MSW. The observed energy spectrum of data/SSM is not significantly distorted, within current errors, though a fit with a distorted spectrum gives a better χ^2 than comparison to the undistorted shape.

The preliminary atmospheric neutrino results are based on 414 live days of data. The double ratios are measured both in the sub-GeV sample and the multi-GeV sample. Both are apparently smaller than unity and consistent with the previous Kamiokande result. Moreover, a large deficit of upgoing ν_μ is observed in the multi-GeV sample. Those anomalies are hard to explain by standard physics and could be evidence of neutrino oscillations. The preliminary results for upward-through-going muons based on 362 days of data are also reported.

The observed zenith angle distribution is still consistent with the no-oscillation expectation within errors. However, it is also consistent with $\nu_\mu \to \nu_x$ oscillation with the parameters suggested by the atmospheric result. Much higher statistics are needed to give a decisive answer for neutrino oscillations.

The parameter region suggested by the atmospheric neutrino results will be explored by the long baseline experiment using a high intensity ν_μ beam from the KEK-PS starting in 1999. We may confirm $\nu_\mu \to \nu_x$ oscillations by detecting a possible distortion of the ν_μ energy spectrum at Super-Kamiokande. It is exciting that oscillations with the parameters $(\Delta m^2, \sin^2 2\theta) \sim (5 \times 10^{-3}, 1)$, which are allowed by both the Kamiokande and the Super-Kamiokande atmospheric neutrino results, cause a large distortion of the ν_μ energy spectrum. Hopefully, we may determine the mode and parameters of neutrino oscillations and open a new field of neutrino physics.

References

[1] The Super-Kamiokande Collaboration: Institute for Cosmic Ray Research (ICRR); University of Tokyo; Gifu University; National Laboratory for High Energy Physics (KEK); Kobe University; Miyagi University of Education; Niigata University; Osaka University; Tokai University; Tokyo Institute of Technology; Tohoku University; Boston University; Brookhaven National Laboratory; University of California, Irvine; California State University, Dominguez Hills; George Mason University; University of Hawaii; Los Alamos National Laboratory; Louisiana State University; University of Maryland; State University of New York at Stony Brook; University of Warsaw; University of Washington.

[2] See, for example, J. N. Bahcall and M. H. Pinsonneault, Rev. Mod. Phys. **67**, 781 (1995).

[3] K. Lande, in *Neutrinos* 96, *Proceedings of the 17th International Conference on Neutrino Physics and Astrophysics*, edited by K. Enqvist *et al.* (Helsinki, Finland, June 1996). See, also, B. T. Cleveland *et al.*, Nucl. Phys. B (Proc. Suppl.) **38**, 47 (1995).

[4] Y. Fukuda *et al.*, Phys. Rev. Lett. **77**, 1683 (1996).

[5] J. N. Abdurashitov *et al.*, Phys. Rev. Lett. **77**, 4708 (1996).

[6] W. Hampel *et al.*, Phys. Lett. B **388**, 384 (1996).

[7] Y. Fukuda *et al.*, preprint ICRR-417-98-13, hep-ex/9805021.

[8] See, for example, N. Hata and P. Langacker, Phys. Rev. D **56**, 6107 (1997), and references therein.

[9] S. P. Mikheyev and A. Yu. Smirnov, Sov. J. Nucl. Phys. **42**, 913 (1985); L. Wolfenstein, Phys. Rev. D **17**, 2369 (1978); *ibid.* **20**, 2634 (1979).

[10] R. Becker-Szendy *et al.*, Phys. Rev. D **46**, 3720 (1992).

[11] R. Clark *et al.*, to be published in Phys Rev. Lett.;
R. Clark, private communication for the $(\mu/\mathrm{e})_{data}/(\mu/\mathrm{e})_{MC}$ value.

[12] Y. Fukuda *et al.*, Phys. Lett. B **335**, 237 (1994).

[13] M. Aglietta *et al.*, Europhys. Lett. **8**, 611 (1989).

[14] K. Daum *et al.*, Z. Phys. C **66**, 417 (1995).

[15] W. W. M. Allison *et al.*, Phys. Lett. B **391**, 491 (1997). M. C. Goodman, for the Soudan-2 Collaboration, talk presented at the Sixth Conference on the Intersections of Particle and Nuclear Physics, Montana, USA, May–June, 1997.

[16] B. Achkar *et al.*, Nucl. Phys. B **434**, 503 (1995).

[17] G. S. Vidyakin *et al.*, Sov. Phys. JETP **71**, 424 (1990); JETP Lett. **59**, 390 (1994).

[18] Chooz Collaboration, preprint hep-ex/9711002 (Nov. 5, 1997).

[19] W. Frati *et al.*, Phys. Rev. D **48**, 1140 (1993).

[20] R. Becker-Szendy *et al.*, Phys. Rev. Lett. **69**, 1010 (1992).

[21] M. Honda *et al.*, Phys. Lett. B **248**, 193 (1990); M. Honda *et al.*, Phys. Rev. D **52**, 4985 (1995).

[22] K. Nishikawa, preprint INS-924 (1992).